

# Masked Image Modeling via Dynamic Token Morphing

Taekyung Kim

Dongyoon Han  
NAVER AI Lab

Byeongho Heo

## Abstract

Masked Image Modeling (MIM) arises as a promising option for Vision Transformers among various self-supervised learning (SSL) methods. The essence of MIM lies in token-wise masked patch predictions, with targets patchified from images; or generated by pre-trained tokenizers or models. We argue targets from the pre-trained models usually exhibit spatial inconsistency, which makes it excessively challenging for the model to follow to learn more discriminative representations. To mitigate the issue, we introduce a novel self-supervision signal based on Dynamic Token Morphing (DTM), which dynamically aggregates contextually related tokens. DTM can be generally applied to various SSL frameworks, yet we propose a simple MIM that employs DTM to effectively improve the performance barely introducing extra training costs. Our experiments on ImageNet-1K and ADE20K evidently demonstrate the superiority of our methods. Furthermore, the comparative evaluation of iNaturalist and Fine-grained Visual Classification datasets further validates the transferability of our method on various downstream tasks. Our code will be released publicly.

## 1. Introduction

Since the success of Vision Transformer (ViT), numerous training strategies have arisen for ViT [13], including self-supervised learning (SSL) methods [6, 8, 15, 16]. Recent advances in masked image modeling (MIM) [17, 47] have established it as a mainstream SSL approach for ViT. In essence, the crux of the MIM methods lies in leveraging token-wise optimization objectives derived from masked patch prediction. Consequently, MIM methods have explored various approaches to generate effective target patches, employing various pre-trained models including vision-language models [4, 28], utilizing momentum teachers [3, 51] or directly exploiting patchified images [17, 47].

However, we observe that patch representations generated by the pre-trained models tend to show *spatial inconsistency* (See §3). Specifically, for example, the patch-wise

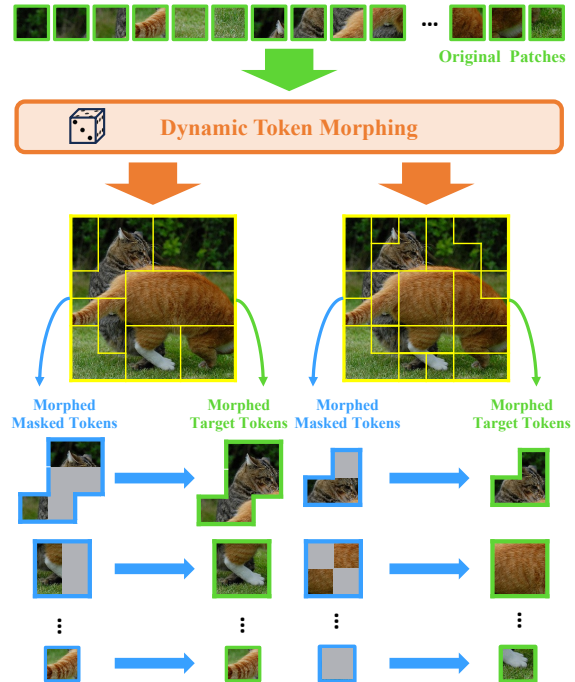


Figure 1. **Dynamic Token Morphing offers contextualized signals.** We illustrate an overview of our Masked Image Modeling via Dynamic Token Morphing (DTM), which aligns the representations of corresponding online and target morphed tokens derived from dynamic aggregation of contextually related tokens. Blue and green boundary denote the representations of the image patches generated by online and target models, respectively. Gray patches represent masked patches.

zero-shot classification of a pre-trained vision-language model reveals spatially inconsistent prediction results, as shown in Fig. 2. To delve deeper into the behaviors of patch representations from pre-trained models, we analyze the impacts of spatial inconsistency from the perspective of discriminability and training capability. We first observe that patch-wise ensemble prediction reveals inferior discriminability in zero-shot image classification and linear probing without token morphing, which aggregates contextually similar tokens. Furthermore, our distillation experiments reveals that token morphing without contextual awareness disrupts pre-training, whereas the model pre-trained using

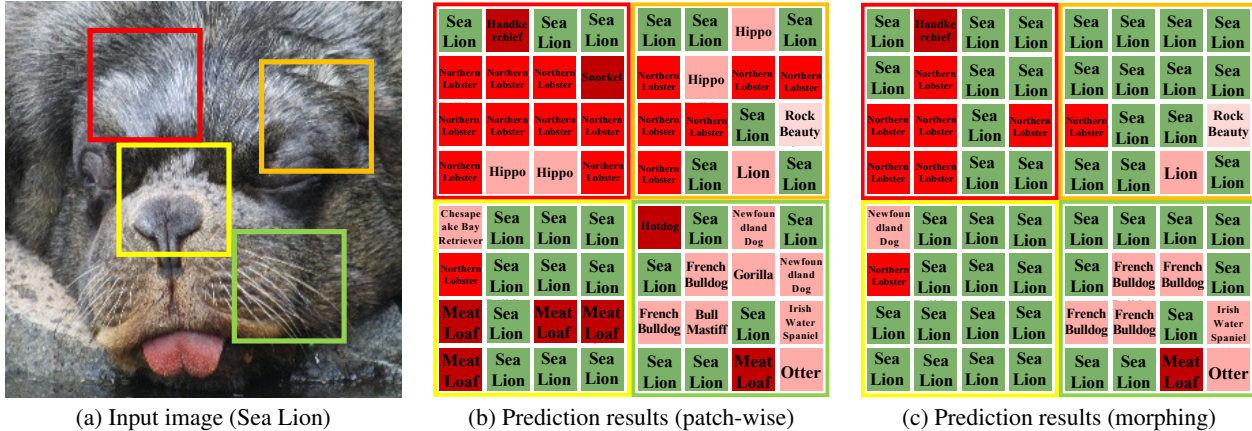


Figure 2. **Visualization of spatial inconsistency.** We present patch-wise prediction results of a sample for zero-shot image classification to visualize the spatially inconsistent predictions among patches. For the given input image in (a), (b) and (c) visualize the predicted classes for each patch in the bounding boxes through patch-wise zero-shot classification with and without token morphing, respectively. Specifically, we depict the differences between the predicted classes and the ground-truth class by varying the lightness of red colors, whereas the darkest green represents the correct prediction. In addition, patch-wise prediction with and without token morphing yields 113 and 82 corrected patches, respectively. We borrow a sea lion image from the ImageNet-V2 dataset [32].

token morphing with context enjoys the potential to enhance representation quality. Consequently, spatially inconsistent target patches pose challenges in learning representations.

Motivated by the observations, we introduce a novel masked image modeling method with our Dynamic Token Morphing (DTM). We conjecture that training should be accelerated by the guidance of composite representations derived from morphed tokens, which aggregate contextually related tokens (see Fig. 1). More specifically, we encode the token-wise target representations and derive matching relations among tokens through DTM. The merging process is performed for both sides of tokens regarding the matching relation and aligning each morphed token with the corresponding merged target tokens. The range of our morphed tokens can vary from a single token to the whole tokens, covering from token-wise to image-level representation learning. We employ the bipartite matching algorithm for token morphing in the aspects of efficiency and efficacy.

Through extensive experiments, we verify the general applicability and scalability of our DTM. We observed that our method improves fine-tuning accuracies across various types of SSL frameworks, affirming its general applicability on SSL methods. Moreover, DTM enhances the baseline from ViT-S/16 to ViT-L/16, demonstrating its scalability. Comparison with previous SSL methods verifying its superiority. Our method shows improved transferability on the iNaturalist and Fine-grained Visual Classification datasets.

## 2. Related Work

**Masked Image Modeling.** Inspired by the promising performance of masked language modeling, BEiT [4] successfully extends the MIM framework into the computer vi-

sion domain, using an external offline tokenizer from DALL-E [30]. iBOT [51] jointly trains the target encoder and the online tokenizer to remove the dependency on the external tokenizer. Data2vec [3] incorporates a momentum encoder to perform feature-level masked prediction tasks, leveraging representations from multiple layers of neural networks. MAE [17] and SimMIM [47] demonstrate efficient masked image modeling by directly reconstructing masked input pixels without any tokenizer. On the other hand, there have been several attempts to exploit the pre-trained model as a tokenizer. BEiT v2 [28] pre-trains a codebook for CLIP [29] to discretize a semantic space. MVP [43] exploits a tokenizer pre-trained with multimodal data to enhance semantics for MIM. A line of studies [33, 44] using CLIP as a teacher to use it as target representations have also been highlighted. Our method aims to utilize a teacher model more effectively, including CLIP, rather than just using it as a raw pre-trained model.

**Token Aggregation Methods.** Token aggregation has mainly been employed to enhance efficiency. Clustering is one of the commonly used token aggregation approaches. Hard clustering methods like K-Means [24], K-Medoids [1], and Density-Peak Clustering with K-Nearest Neighbors (DPC-KNN) enforce each data to exclusively belong to a single cluster. Bipartite matching [19] also aggregates data in a hard clustering manner, optimizing pairs of elements from two disjoint sets given objective function. Soft clustering allows data to belong to multiple clusters. LIT [27] employs deformable token merging layers to aggregate tokens between stages. Furthermore, some token pruning methods [23, 31, 35, 48] can be categorized as token aggregation methods; however, they have deeply fo-

| Token morphing | Zero-shot image classification (%) | Linear probing (%) |
|----------------|------------------------------------|--------------------|
|                | 26.5                               | 73.2               |
| ✓              | 30.8 (+4.3)                        | 77.6 (+3.2)        |

Table 1. **Analysis on the impacts of handling spatial inconsistency.** We quantitatively compare the patch-wise ensemble prediction with and without token morphing. We evaluate the accuracies for linear probing on ImageNet-1K. We conduct linear probing for 25 epochs. We fix the number of smoothing tokens by half of the whole tokens.

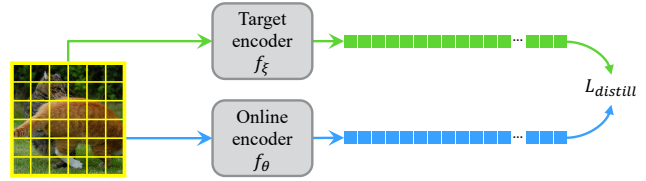
cused on compressing tokens to achieve a cost-efficient vision transformer. While the above token aggregation methods have mainly been employed to boost efficiency, our approach diverges significantly. We leverage the concept of token aggregation to address spatial inconsistency in patch-level supervision, thereby enhancing the effectiveness of masked image modeling in terms of precision.

### 3. Motivation

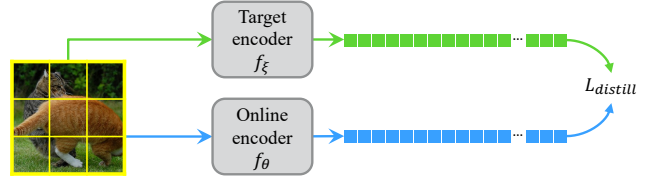
In this section, we study the spatially inconsistent behavior of patch representations generated by pre-trained models and its impacts on pre-training. We visualize the spatial inconsistency of patch representations from a vision-language model in Fig. 2. Then, we conduct a quantitative analysis of the spatial inconsistency on the dataset scale in Table 1. Finally, we compare the distillation capability among token-wise, down-sampling-based, and several token aggregation-based objectives to confirm the efficacy of representation learning via context-aware token morphing.

**Visualization of spatial inconsistent predictions.** To verify the spatial inconsistency among patch representations of the pre-trained model, we attempt to investigate spatially inconsistent predictions among patches through patch-wise zero-shot classification. To emphasize the spatial inconsistent representations, we conduct a comparative analysis between vanilla patch-wise prediction and prediction with smoothed tokens through token morphing, which aggregates contextually related tokens. Given the input image in Fig. 2a, we visualize the patch-wise prediction results with and without token morphing in Fig. 2b and 2c, respectively. Here, patches with accurate predictions are colored in green, while misclassified patches are colored in red. The wrong patches gradually transition to a darker red as the predicted class deviates from the ground-truth class.

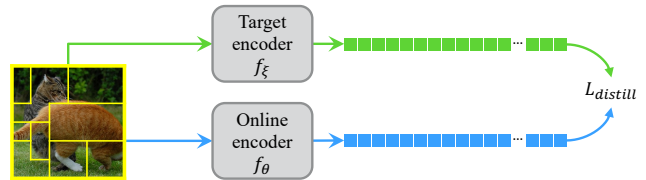
Utilizing token morphing for predictions yields improved accuracy with 113 correct patches out of 196 and a gap of 31 patches compared to vanilla patch-wise prediction, demonstrating the importance of spatial consistency. On the other hand, despite the proximity and contextual similarity among patches, the wrong patches in the green



(a) Token-wise distillation (baseline)



(b) Distillation with downsampled supervisions



(c) Distillation with token aggregations

Figure 3. **Various supervision configurations for distillation.** We depict the different self-supervision signals between token-wise distillation, distillation with downsampled supervisions, and distillation with token aggregations.

| Distillation signals              | Linear probing (%) |
|-----------------------------------|--------------------|
| Token-wise (baseline)             | 70.9               |
| Downsampling                      | 68.8 (-2.1)        |
| Layer-wise Bipartite Matching [5] | 70.2 (-0.7)        |
| Dynamic Token Morphing (Ours)     | 72.2 (+1.3)        |

Table 2. **Comparison on distillation capacity varying distillation configuration.** We evaluated linear probing accuracies of various distillation approaches. The distillation configurations are illustrated in Fig. 3. We pre-train for 50 epochs and perform linear probing for 50 epochs on ImageNet-1K [34].

box (bottom right) in Fig. 2b exhibit spatially inconsistent prediction results (french bulldog, gorilla, bull mastiff, hotdog, and newfoundland dog) while patches in Fig 2c show correct or relatively consistent predictions (french bulldog). The comparison between the two prediction results highlights the spatially inconsistent representations among patches of the pre-trained models, potentially disrupting representation learning when used as targets.

**Analysis of the impact of spatial inconsistency.** To quantitatively assess the impacts of spatial inconsistency on the dataset scale, we conduct a quantitative comparison

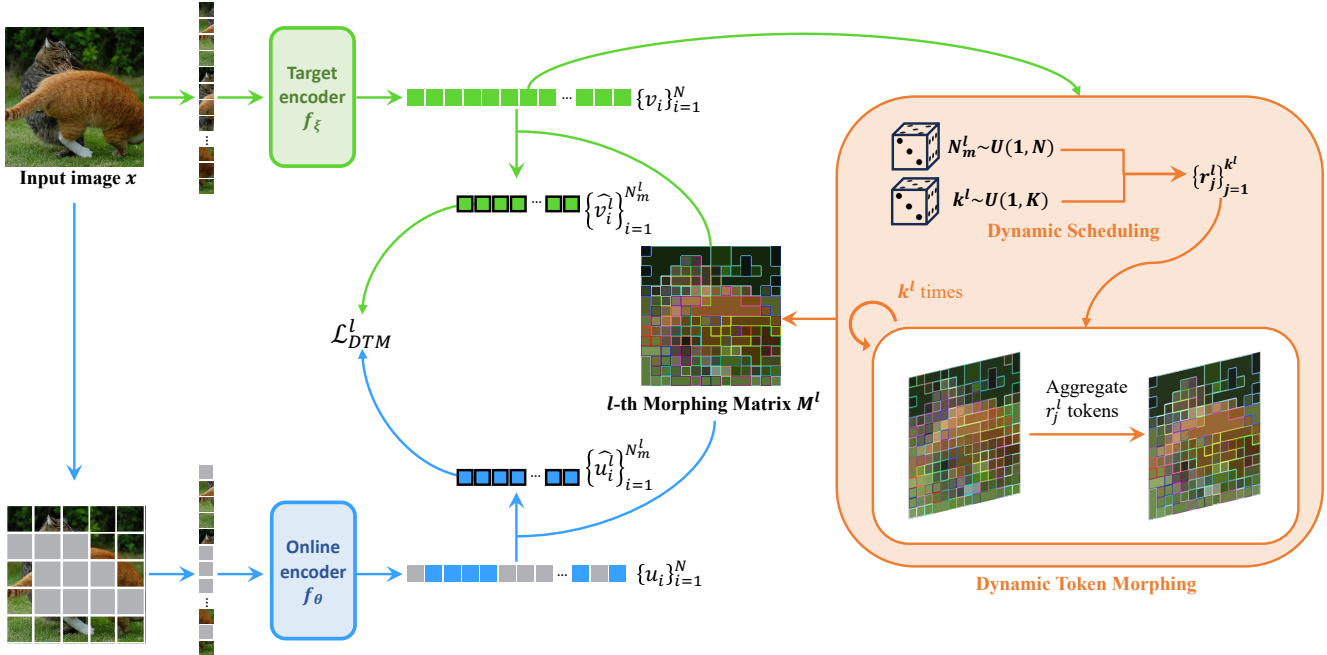


Figure 4. **Framework overview of our Masked Image Modeling via Dynamic Token Morphing.** We introduce a simple framework that performs Masked Image Modeling (MIM) tasks via Dynamic Token Morphing (DTM). For the  $l$ -th DTM, we aggregate dynamic range of tokens using  $l$ -th morphing matrix  $M^l$  derived from target tokens  $\{v_i\}_{i=1}^N$ . Specifically, we randomly sample final number of morphed tokens  $N_m^l$  and an iteration number  $k^l$  to dynamically schedule token morphing (i.e.,  $\{r_j^l\}_{j=1}^{k^l}$ ), eventually forming  $N_m^l$  morphed tokens  $\{\hat{v}_i\}_{i=1}^{N_m^l}$ . Then, we align representations of the corresponding online and target morphed tokens. Note that our baseline is identical to our framework except for dynamic token morphing, which we compared with in Section 5. We use a cat image from ImageNet-1K.

between patch-wise ensemble predictions with and without token morphing. Specifically, in the case of patch-wise ensemble prediction without token morphing, we predict the class scores for each patch and average the scores across the patches within the given image. In contrast, in the case of token morphing, we aggregate groups of semantically associated tokens and average the token representations group-wise before patch-wise ensemble prediction. We use the CLIP Base model for the encoder. We aggregate 98 tokens for token morphing, which occupy half of all tokens. Table 1 reports zero-shot image classification and linear probing results on ImageNet-1k. Patch-wise ensemble prediction with token morphing exceeds the performances without token morphing, which reveals that patch representations exhibit spatial inconsistency, and the token morphing for contextually related tokens can remedy the inconsistency.

#### Comparison on distillation capability varying learning objectives.

We further conduct a quantitative comparison of distillation approaches with varying configurations, as described in Fig. 3. The goal is to demonstrate the importance of resolving spatial inconsistency for representation learning while showing that indiscriminate aggregation may risk degrading the representations. We compare

token-wise distillation, distillation with downsampled supervisions, distillation with layer-wise Bipartite Matching during encoding for targets, and distillation with our Dynamic Token Morphing. For each configuration, we pre-train ViT-B/16 for 50 epochs and perform linear probing for 50 epochs on ImageNet-1K. As shown in Table 2, distillation with token morphing exceeds the performance of the token-wise distillation approach, revealing that patch representations exhibit spatial inconsistency, and token morphing for contextually related tokens can remedy this inconsistency. However, since the downsampling approach aggregates tokens without context awareness, and the layer-wise Bipartite Matching approach has a risk of harming final representations during encoding, both approaches exhibit degraded performances. The results emphasize the importance of context-aware token morphing.

## 4. Method

We introduce a novel masked image model training based on our Dynamic Token Morphing (DTM). In DTM, we analyze the relation between token representations and aggregate similar tokens to build morphed tokens representing various semantic information. By aligning morphed to-

| Framework                     | Method           | FT. (%)     |
|-------------------------------|------------------|-------------|
| Feature MIM<br>(CLIP teacher) | MAE + CLIP       | 82.6        |
|                               | MAE + CLIP + DTM | 83.2 (+0.6) |
|                               | BEiT v2          | 84.2        |
|                               | BEiT v2 + DTM    | 84.4 (+0.2) |
| Image-level SSL               | BYOL             | 81.7        |
|                               | BYOL + DTM       | 82.1 (+0.4) |

Table 3. **Applicability of Dynamic Token Morphing (DTM) on various SSL frameworks.** We compared the fine-tuning accuracies between models pre-trained by the vanilla SSL method and DTM. We adopted MAE [17] with CLIP teacher [29], BEiT v2 [28], and BYOL [15] to cover general SSL frameworks. We employed the ViT-B/16 architecture with a resolution of  $224 \times 224$ . All the models are pre-trained for 100 epochs.

kens from online and target encoders, the masked image model is applied in morphed token-level rather than token-level loss of conventional methods. DTM is designed for universal application across various online and target encoders. The framework of DTM is described in Fig. 4, where the DTM module is straightforwardly added to the baseline MIM scheme.

#### 4.1. Token Encoding Process Formulation

We begin by formulating the token encoding process. Given an image  $x$ , we patchify the image into  $N$  patches  $\{x_i\}_{i=1}^N$ . We select positions  $\mathcal{M} \subset \{1, 2, \dots, N\}$  of masked patches in a block-wise manner with a masking ratio  $r \in (0, 1)$  so that  $|\mathcal{M}| = \lfloor rN \rfloor$ . We mask the image patches by replacing the image patches of the position in  $\mathcal{M}$  to a shared learnable embedding  $e_{[M]}$ . To this end, the input of the encoders becomes  $\{x_i^M\}_{i=1}^N$  where  $x_i^M = e_{[M]}$  for  $i \in \mathcal{M}$  and  $x_i^M = x_i$  for  $i \notin \mathcal{M}$ . The masked patches  $\{x_i^M\}_{i=1}^N$  are concatenated with a learnable CLS token  $e_{[CLS]}$  and fed into the online encoder  $f_\theta$  with a subsequent linear head  $h_\theta$  and the target encoder  $f_\xi$ , and become encoded online tokens  $\{u_i\}_{i=1}^N$  and  $\{v_i\}_{i=1}^N$  where  $u_i = h_\theta(f_\theta(x_i^M))$  and  $v_i = f_\xi(x_i^M)$ , respectively.

#### 4.2. Dynamic Token Morphing

Considers  $l$ -th DTM among total  $L$  levels DTM, dynamic token morphing scheduling randomly assigns  $N_m^l$  number of final morphed tokens and  $k_l$  number of iterations to aggregate tokens. Then, we compute token morphing schedule  $R^l = \{r_j^l\}_{j=1}^{k^l}$ , a sequence of token numbers  $r_j^l$  to aggregate. Rather than samples a sequence of random numbers  $r_j^l$  that satisfy  $\sum_{j=1}^{k^l} r_j^l = N - N_m^l$ , we simply define  $r_j^l$  as:

$$r_j^l = \begin{cases} \lfloor (N - N_m^l)/k^l \rfloor, & \text{if } j < k^l \\ N - (k^l - 1)\lfloor (N - N_m^l)/k^l \rfloor, & \text{otherwise.} \end{cases} \quad (1)$$

| Method         | ViT-S  | ViT-B  | ViT-L  |
|----------------|--------|--------|--------|
| MIM (Baseline) | 82.7   | 84.3   | 86.4   |
| DTM (Ours)     | 83.1   | 85.4   | 86.7   |
| Gain           | (+0.4) | (+1.1) | (+0.3) |

Table 4. **Validation of the proposed method varying scales of the backbone architecture.** We evaluated the improvements in fine-tuning accuracies between the baseline and our method for ViT-S/16, ViT-B/16, and ViT-L/16 with a resolution of  $224 \times 224$ . All the models are pre-trained for 300 epochs.

At this point, the token morphing function  $\phi_{R^l}^l(\cdot)$  for the  $l$ -th level contextual representations can be determined by  $R^l$ . Note that each  $l$ -th level token morphing function  $\phi^l$  is dynamically changed based on randomly sampled  $N_m^l$  and  $k_l$ . Eventually, we can obtain the  $l$ -th level token morphing matrix  $M^l = [m_{ij}^l]$ , a contextual relation among tokens, from the target token representation  $\{v_i\}_{i=1}^N$  as follows:

$$M^l = \phi^l(\{v_i\}_{i=1}^N), \quad (2)$$

where  $m_{ij} = 1$  indicates the aggregation of the  $j$ -th token  $v_j$  to the  $i$ -th token  $v_i$ . In addition, every token is assigned to a specific cluster, even in cases where it forms a single token cluster, and each token retains its exclusive association with a single cluster. Thus, morphing matrix  $M^l = [m_{ij}^l]$  should satisfy the following two conditions,  $\sum_i \sum_j m_{ij} = N$  and  $\sum_i m_{ij} = 1$ . Our DTM is universal to any token aggregation method; we simply employ bipartite matching to efficiently search for contextually similar tokens.

Based on the  $l$ -th level token morphing matrix  $M^l$  obtained from dynamic token morphing, the representations for online and target morphed tokens can be derived by:

$$\begin{aligned} \widehat{u}_i^l &= \sum_j m_{ij}^l u_j^l, \\ \widehat{v}_i^l &= \sum_j m_{ij}^l v_j^l, \end{aligned} \quad (3)$$

where  $\{\widehat{u}_i^l\}_{i=1}^{N_m^l}$  and  $\{\widehat{v}_i^l\}_{i=1}^{N_m^l}$  denote for the representations of online and target morphed tokens, respectively.

#### 4.3. Training Objective

We formulate the objective function by accumulating DTM loss, which aligns the representations of the corresponding online and target morphed tokens derived by DTM. The DTM loss can be formulated as follows:

$$\mathcal{L}_{\text{DTM}}^l = \sum_{i=1}^{N_m^l} w_i d_i(\widehat{u}_i^l, \widehat{v}_i^l), \quad (4)$$

where  $d_i$  is the  $i$ -th distance function,  $w_i = \sum_j m_{ij}$  is a number of aggregated tokens for the  $i$ -th online and target

| Method                        |            | Pre-training epochs |       |       | Supervision     | ViT-S       | ViT-B       | ViT-L       | Seg.        |
|-------------------------------|------------|---------------------|-------|-------|-----------------|-------------|-------------|-------------|-------------|
|                               |            | ViT-S               | ViT-B | ViT-L |                 |             |             |             |             |
| <i>Supervised models</i>      |            |                     |       |       |                 |             |             |             |             |
| DeiT [37]                     | ICML 2021  | -                   | -     | -     | Label           | -           | 81.8        | -           | -           |
| DeiT-III [38]                 | ECCV 2022  | -                   | -     | -     | Label           | -           | 83.8        | 84.2        | 49.3        |
| Cosub [39]                    | CVPR 2023  | -                   | -     | -     | Label           | 81.5        | 84.2        | 85.3        | 49.3        |
| <i>Self-supervised models</i> |            |                     |       |       |                 |             |             |             |             |
| MoCo v3 [9]                   | ICCV 2021  | 300                 | 300   | 300   | Pixel           | 81.7        | 83.2        | 84.1        | 47.3        |
| BEiT [4]                      | ICLR 2021  | 300                 | 800   | 800   | DALL-E          | 81.7        | 83.2        | 85.2        | 47.1        |
| DINO [6]                      | ICCV 2021  | 3200                | 1600  | -     | Feature         | 82.0        | 83.6        | -           | 46.8        |
| SplistMask [14]               | arXiv 2021 | 300                 | 300   | -     | Pixel + Feature | 81.5        | 83.6        | -           | 46.8        |
| iBOT [51]                     | ICLR 2022  | 3200                | 1600  | 1000  | Feature         | 82.3        | 84.0        | 84.8        | 50.0        |
| MAE [17]                      | CVPR 2022  | -                   | 1600  | 1600  | Pixel           | -           | 83.7        | 85.6        | 48.1        |
| SimMIM [47]                   | CVPR 2022  | -                   | 800   | -     | Pixel           | -           | 83.8        | -           | -           |
| MaskFeat [42]                 | CVPR 2022  | -                   | 1600  | 1600  | Feature         | -           | 84.0        | 85.7        | -           |
| ExtreMa [45]                  | arXiv 2022 | -                   | 300   | -     | Feature         | -           | 83.7        | -           | 47.9        |
| CAE [10]                      | arXiv 2022 | 300                 | 1600  | 1600  | Pixel + Feature | 82.0        | 83.9        | 86.3        | 50.2        |
| CMAE [18]                     | arXiv 2022 | -                   | 1600  | 1600  | Pixel + Feature | -           | 84.4        | 85.3        | 50.1        |
| FD-CLIP [44]                  | arXiv 2022 | -                   | 300   | -     | CLIP B/16       | -           | 84.9        | -           | 52.8        |
| BEiT v2 [28]                  | arXiv 2022 | -                   | 300   | 300   | CLIP B/16       | -           | 85.0        | 86.6        | 52.7        |
| data2vec [3]                  | ICML 2022  | -                   | 800   | 1600  | Feature         | -           | 84.2        | 86.6        | -           |
| mc-BEiT [22]                  | ECCV 2022  | -                   | 800   | 800   | VQGAN           | -           | 84.1        | 85.6        | 47.0        |
| MVP [43]                      | ECCV 2022  | -                   | 300   | 300   | CLIP B/16       | -           | 84.4        | 86.3        | 52.4        |
| SdAE [11]                     | ECCV 2022  | -                   | 300   | -     | Pixel           | -           | 84.1        | -           | 48.6        |
| MSN [2]                       | ECCV 2022  | -                   | 600   | -     | Feature         | -           | 83.4        | -           | -           |
| BootMAE [12]                  | ECCV 2022  | -                   | 800   | 800   | Pixel + Feature | -           | 84.2        | 85.9        | 49.1        |
| CAN [25]                      | arXiv 2023 | -                   | 1600  | 800   | Pixel           | -           | 83.6        | 84.7        | -           |
| SemMAE [21]                   | NIPS 2022  | -                   | 800   | -     | Pixel           | -           | 83.3        | -           | 46.3        |
| ConMIM [49]                   | ICLR 2023  | 300                 | 800   | 1600  | Dictionary      | 79.8        | 83.7        | 85.5        | 46.0        |
| RC-MAE [49]                   | ICLR 2023  | 1600                | 1600  | 1600  | Pixel           | 82.0        | 83.6        | 86.1        | -           |
| MixedAE [7]                   | CVPR 2023  | -                   | 1600  | -     | Pixel           | -           | 83.9        | -           | 49.8        |
| SIM [36]                      | CVPR 2023  | -                   | 1600  | -     | Feature         | -           | 83.8        | -           | -           |
| HPM [41]                      | CVPR 2023  | -                   | 800   | 800   | Pixel           | -           | 84.2        | 85.8        | 48.5        |
| DeepMIM [33]                  | arXiv 2023 | -                   | 300   | -     | CLIP B/16       | -           | 84.8        | -           | -           |
| DTM (Ours)                    | -          | 300                 | 300   | 300   | CLIP B/16       | <b>83.2</b> | <b>85.4</b> | <b>86.7</b> | <b>53.1</b> |

Table 5. **Comparisons with previous models on ImageNet-1K.** We compare All models were pre-trained and fine-tuned on ImageNet-1K. We evaluate the improvements in fine-tuning accuracies between the baseline and our method for ViT-S/16, ViT-B/16, and ViT-L/16 with a resolution of  $224 \times 224$ . All our models are pre-trained for 300 epochs, which reveals the cost-efficiency in training. We further show ADE20K semantic segmentation results for each model trained by the standard training protocol.

morphed tokens. Note that our DTM loss can be extended to token-wise or image-level losses when  $N_m^l = N$  or  $N_m^l = 1$ , respectively. We adopt Cosine distance for the distance function in Eq. (4) for all the DTM losses. Therefore, the final objective function is the summation of all DTM losses, which is defined as:

$$\min_{\theta} \sum_{l=1}^L \mathcal{L}_{\text{DTM}}^l. \quad (5)$$

## 5. Experiment

**Pre-training setup.** We use the training dataset of ImageNet-1K for pre-training. We pre-train our framework

and other SSL frameworks through DTM on ImageNet-1K. We pre-train our framework with ViT-S/16, ViT-B/16, and ViT-L/16 for 300 epochs using AdamW with momentum (0.9, 0.98) and a batch size of 1024. We use a learning rate of  $1.5 \times 10^{-4}$  with cosine decay and warmup 10 epochs. We employ the CLIP base model with its visual projector as a target model across all scales of ViT. Block-wise masking is used with a ratio of 0.4. Cosine distance is used as a distance metric for the objective according to an ablation study in Appendix. We also pre-train various SSL frameworks through our DTM. Detailed pre-training setups can be found in Appendix. All models are pre-trained using 8 V100-32GB GPUs.

| Method     | Birds           | CUB-200         | CIFAR-10        | CIFAR-100       | Dogs            | Average     |
|------------|-----------------|-----------------|-----------------|-----------------|-----------------|-------------|
| Baseline   | 87.3 (86.5±0.6) | 87.1 (86.8±0.6) | 99.2 (99.1±0.0) | 92.0 (91.9±0.3) | 86.9 (86.8±0.1) | 90.5        |
| DTM (Ours) | 88.8 (88.2±0.4) | 88.8 (88.1±0.4) | 99.3 (99.2±0.0) | 92.3 (92.1±0.2) | 87.9 (87.8±0.2) | 91.4 (+0.9) |

Table 6. **Transfer learning results on Fine-Grained Visual Classification (FGVC) datasets.** We present the end-to-end fine-tuning accuracies on multiple datasets, reporting the best results along with the mean  $\pm$  std of the accuracies from grid searches. Our Dynamic Token Morphing (DTM) outperforms the baseline at the best accuracies overall.

| Method     | iNat 2018              | iNat 2019              | iNat 2021-mini         |
|------------|------------------------|------------------------|------------------------|
| Baseline   | 75.0 (74.6±0.6)        | 81.1 (79.8±1.0)        | 75.8 (75.2±0.6)        |
| DTM (Ours) | <b>78.5 (77.4±0.6)</b> | <b>81.9 (81.2±0.6)</b> | <b>78.4 (77.5±0.6)</b> |

Table 7. **Transfer learning results on iNaturalists.** We further present the end-to-end fine-tuning accuracies on the iNaturalist 2018, iNaturalist 2019, and mini iNaturalist 2021 datasets [40]. We report the best results along with the mean  $\pm$  std of the set of accuracies obtained from grid searches for each method. Our method consistently outperforms the competitors in terms of the best accuracies, further showcasing remarkable tuning robustness.

**Fine-tuning setup.** We fine-tune our pre-trained models on ImageNet-1K [34] by default. Pre-trained ViT-S, ViT-B, and ViT-L are fine-tuned for 300, 100, and 50 epochs, respectively. The pre-trained models are optimized by AdamW with a weight decay of 0.05. We use a layer-wise learning rate decay of 0.6 for ViT-S and ViT-B and 0.8 for ViT-L. Learning rate is set to  $5 \times 10^{-4}$  with a linear warmup for 10 epochs for ViT-S and ViT-B and 5 epochs for ViT-L. Additional fine-tuning details are listed in Appendix.

### 5.1. Effectiveness of Our Method

**Applicability.** We apply DTM on BEiT v2, MAE with the CLIP teacher [29], and BYOL [15] to verify its applicability to various SSL frameworks. As shown in Table 3, our DTM successfully improves the fine-tuning accuracy of MAE + CLIP, BEiT v2, and BYOL by 0.5%p, 0.2%p, and 0.4%p, which reveals its general applicability on various frameworks beyond our baseline.

**Scalability.** We further study the scalability of DTM. We compare the fine-tuning accuracies of our method to its baseline, which is pre-trained without DTM. We pre-train ViT-S/16, ViT-B/16, and ViT-L/16 with a resolution of  $224 \times 224$  for each method and evaluate the performance gains in fine-tuning accuracies. As shown in Table 5, DTM improved ViT-S/16, ViT-B/16, and ViT-L/16 by 0.4%p, 1.1%p, and 0.3%p, respectively, verifying its general efficacy across different scales.

### 5.2. ImageNet-1K Classification

We compare the fine-tuning accuracy of our method with previous state-of-the-art self-supervised methods on ImageNet-1K [34] datasets. The comparisons include su-

| Method   | $\mathcal{L}_{\text{Token\_Morphing}}$ | Dynamic | FT. (%)           |
|----------|--|---------|-------------------|
| Baseline | -                                      | -       | 84.3              |
| DTM      | ✓                                      | -       | 84.0 (-0.3)       |
| DTM      | ✓                                      | ✓       | <b>85.4(+1.1)</b> |

Table 8. **Ablation study on dynamic mechanism.** We investigate the efficacy of the dynamic mechanism in DTM, revealing its significant contribution to our method.

pervised learning and SSL methods with various supervision signals. In the case when the target model is CLIP, we only compare models pre-trained with CLIP B/16 for 300 epochs for fair comparison. Table 5 reports the fine-tuning accuracies of ViT-S/B/L backbones. We observe that our MIM pre-trained by DTM achieves 83.2%, 85.4%, 86.7% top-1 accuracy with ViT-S/16, ViT-B/16, and ViT-L/16, which outperforms state-of-the-art performances across the scales. Specifically, our method surpasses MVP, DeepMIM, and BEiT v2 by 1.0%p, 0.6 %p, and 0.4%p on ViT-B/16, respectively. Moreover, our method definitely outperforms other methods that leverage supervisions other than CLIP representations, which demonstrates the superiority of our method among self-supervised learning methods.

### 5.3. ADE20K Semantic Segmentation

We further evaluate semantic segmentation performances on ADE20K [50] to verify the transferability of our pre-trained model to dense prediction tasks. We follow the training and evaluation protocol [17]; the models are fine-tuned for 160K iterations using UperNet [46] with a batch size of 16 and a resolution of  $512 \times 512$ . We initialize UperNet with our pre-trained ViT-B/16. Detailed hyperparameters for semantic segmentation fine-tuning can be found in Appendix. The first right column in Table 5 shows the mIoU performance comparison. Our method also outperforms the previous state-of-the-art results with a margin of 0.3%p, validating its superiority over other SSL methods. This result signifies that our method is effective in enhancing discriminability for dense prediction tasks.

### 5.4. Transfer learning

**iNaturalist datasets.** We verify the improved transferability of our pre-trained model. We compare fine-tuning accuracies of the baseline and our proposed model on iNatu-

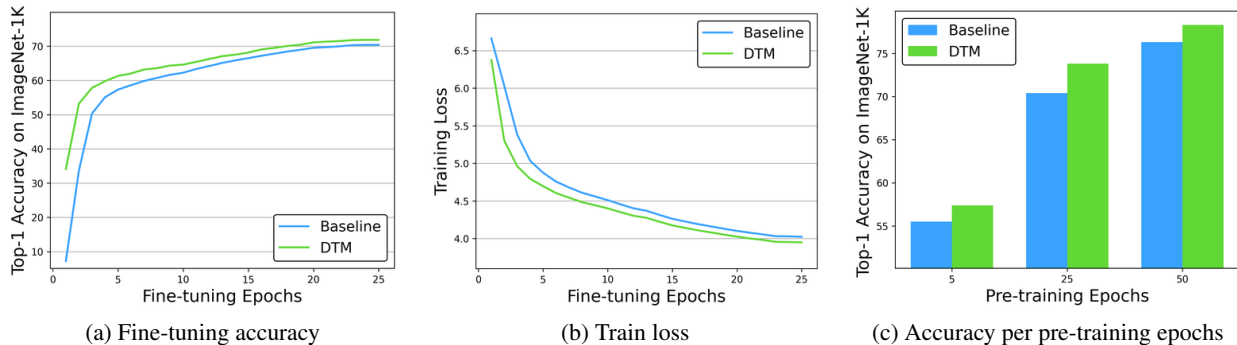


Figure 5. **Training trends visualizations.** We plot (a) top-1 accuracies and (b) training losses during fine-tuning on ImageNet-1K for models pre-trained by Dynamic Token Morphing (DTM) versus its baseline. (c) confirms the impact of pre-training epochs for DTM over the baseline. We use the ViT-B/16 architectures with a resolution of  $224 \times 224$ . In both (a) and (b), DTM consistently exhibits a substantial gap compared to the baseline during the entire fine-tuning phase, indicating that DTM inherently benefits from stronger supervision, facilitating the training process. DTM shows consistency in improving the baseline regardless of the pre-training epochs, as shown in (c).

realist 2018, iNaturalist 2019, and mini iNaturalist 2021 [40], which are highly imbalanced with different numbers of images per class. All the models are ViT-B/16 with a resolution of  $224 \times 224$ . Following the protocol [20], we perform grid searches on learning rates and weight decay and report the maximum accuracy and the mean and standard deviation of the accuracies. Table 7 shows our DTM loss significantly improves the baseline with large margins, which reveals enhanced transferability.

#### Fine-Grained Visual Classification (FGVC) datasets.

We further validate the transferability of our method. Following the evaluation protocol as above, we conduct comparisons on FGVC datasets. Specifically, we evaluate fine-tuning accuracies on Birds, CUB-200, CIFAR-10, CIFAR-100, and Dogs through grid searches with different learning rates and weight decays. As shown in Table 6, our method outperforms the baseline overall across the datasets, which shows superior transferability and tuning robustness.

#### 5.5. Analysis

**Ablation study on the importance of dynamics.** Table 8 presents an ablation study on the effectiveness of the dynamic mechanism on DTM. We employ a ViT-B/16 model with a resolution of  $224 \times 224$ . The models are pre-trained for 300 epochs and fine-tuned for 100 epochs on ImageNet-1K [34]. For token morphing without the dynamic mechanism, half of the total 196 tokens are aggregated for each image. As shown in Table 8, token morphing with dynamic mechanism significantly improves the baseline while performance degrades without the dynamic mechanism, which demonstrates the importance of dynamic mechanism in DTM.

**Faster convergence.** We analyze the behaviors of models pre-trained by DTM and token-wise objectives in Fig. 5. All

the approaches employ CLIP representations for the target. As shown in Fig. 5a, the fine-tuning accuracies of DTM surpass the accuracy of the token-wise supervision approaches. Fig. 5b shows that the model pre-trained by DTM exhibits a lower fine-tuning loss compared to the baseline model, verifying better convergence. Finally, Fig. 5c verifies consistent effect of DTM across various pre-training epochs.

## 6. Conclusion

We have introduced a novel masked image modeling method with morphed tokens to address the negative impacts of spatially inconsistent target representations during pre-training. We first analyze the existence and impacts of spatial inconsistency in target representations. Specifically, we qualitatively observed spatial inconsistency among patches from pre-trained models despite proximity and contextual similarity. Then, we investigate the impacts on downstream tasks, including zero-shot image classification and linear classification. We further validate that token morphing enhances the pre-training capability of the target patches, while arbitrary aggregation, like downsampling, tends to disrupt them. The results demonstrate the necessity of token morphing to alleviate spatial inconsistency. Based on the observation, we have proposed Dynamic Token Morphing, dynamically aggregating contextually associated tokens with a random number of matching tokens. Subsequently, our method aligns the representations of morphed tokens with the representations of their corresponding morphed targets. The extensive experiments verify its general applicability, scalability, and superiority. We further validate its transferability on the iNaturalist datasets and Fine-grained Visual Classification datasets. Subsequent analysis reveals superiority over the baseline.



**Limitation** Despite the potential of our method, we have verified its applicability only up to ViT-L/16. Resource limitations prevented us from performing more experiments on larger-scale models such as ViT-G. We will explore this in our future work.

## References

- [1] *Partitioning Around Medoids (Program PAM)*, chapter 2, pages 68–125. John Wiley & Sons, Ltd, 1990. [2](#)
- [2] Mahmoud Assran, Mathilde Caron, Ishan Misra, Piotr Bojanowski, Florian Bordes, Pascal Vincent, Armand Joulin, Michael Rabbat, and Nicolas Ballas. Masked siamese networks for label-efficient learning. *arXiv preprint arXiv:2204.07141*, 2022. [6](#)
- [3] Alexei Baevski, Wei-Ning Hsu, Qiantong Xu, Arun Babu, Jiatao Gu, and Michael Auli. data2vec: A general framework for self-supervised learning in speech, vision and language. In *International Conference on Machine Learning*, pages 1298–1312. PMLR, 2022. [1](#), [2](#), [6](#)
- [4] Hangbo Bao, Li Dong, Songhao Piao, and Furu Wei. Beit: Bert pre-training of image transformers. In *International Conference on Learning Representations*, 2021. [1](#), [2](#), [6](#)
- [5] Daniel Bolya, Cheng-Yang Fu, Xiaoliang Dai, Peizhao Zhang, Christoph Feichtenhofer, and Judy Hoffman. Token merging: Your vit but faster. *arXiv preprint arXiv:2210.09461*, 2022. [3](#)
- [6] Mathilde Caron, Hugo Touvron, Ishan Misra, Hervé Jégou, Julien Mairal, Piotr Bojanowski, and Armand Joulin. Emerging properties in self-supervised vision transformers. In *Proceedings of the International Conference on Computer Vision*, 2021. [1](#), [6](#)
- [7] Kai Chen, Zhili Liu, Lanqing Hong, Hang Xu, Zhen-guo Li, and Dit-Yan Yeung. Mixed autoencoder for self-supervised visual representation learning. In *Proceedings of the IEEE/CVF Conference on Computer Vision and Pattern Recognition (CVPR) (CVPR)*, pages 22742–22751, 2023. [6](#)
- [8] Ting Chen, Simon Kornblith, Mohammad Norouzi, and Geoffrey Hinton. A simple framework for contrastive learning of visual representations. *arXiv preprint arXiv:2002.05709*, 2020. [1](#)
- [9] Xinlei Chen, Saining Xie, and Kaiming He. An empirical study of training self-supervised vision transformers. *arXiv preprint arXiv:2104.02057*, 2021. [6](#)
- [10] Xiaokang Chen, Mingyu Ding, Xiaodi Wang, Ying Xin, Shentong Mo, Yunhao Wang, Shumin Han, Ping Luo, Gang Zeng, and Jingdong Wang. Context autoencoder for self-supervised representation learning. *arXiv preprint arXiv:2202.03026*, 2022. [6](#)
- [11] Yabo Chen, Yuchen Liu, Dongsheng Jiang, Xiaopeng Zhang, Wenrui Dai, Hongkai Xiong, and Qi Tian. Sdae: Self-distilled masked autoencoder. In *European Conference on Computer Vision*, pages 108–124. Springer, 2022. [6](#)
- [12] Xiaoyi Dong, Jianmin Bao, Ting Zhang, Dongdong Chen, Weiming Zhang, Lu Yuan, Dong Chen, Fang Wen, and Nenghai Yu. Bootstrapped masked autoencoders for vision bert pretraining. *arXiv preprint arXiv:2207.07116*, 2022. [6](#)
- [13] Alexey Dosovitskiy, Lucas Beyer, Alexander Kolesnikov, Dirk Weissenborn, Xiaohua Zhai, Thomas Unterthiner, Mostafa Dehghani, Matthias Minderer, Georg Heigold, Sylvain Gelly, Jakob Uszkoreit, and Neil Houlsby. An image is worth 16x16 words: Transformers for image recognition at scale. In *International Conference on Learning Representations*, 2021. [1](#)
- [14] Alaaeldin El-Nouby, Gautier Izacard, Hugo Touvron, Ivan Laptev, Hervé Jegou, and Edouard Grave. Are large-scale datasets necessary for self-supervised pre-training? *arXiv preprint arXiv:2112.10740*, 2021. [6](#)
- [15] Jean-Bastien Grill, Florian Strub, Florent Altché, Corentin Tallec, Pierre Richemond, Elena Buchatskaya, Carl Doersch, Bernardo Avila Pires, Zhaohan Guo, Mohammad Gheshlaghi Azar, Bilal Piot, koray Kavukcuoglu, Remi Munos, and Michal Valko. Bootstrap Your Own Latent - A New Approach to Self-Supervised Learning. In *Advances in Neural Information Processing Systems*, pages 21271–21284. Curran Associates, Inc., 2020. [1](#), [5](#), [7](#)
- [16] Kaiming He, Haoqi Fan, Yuxin Wu, Saining Xie, and Ross Girshick. Momentum contrast for unsupervised visual representation learning. *arXiv preprint arXiv:1911.05722*, 2019. [1](#)
- [17] Kaiming He, Xinlei Chen, Saining Xie, Yanghao Li, Piotr Dollár, and Ross Girshick. Masked autoencoders are scalable vision learners. In *Proceedings of the IEEE/CVF Conference on Computer Vision and Pattern Recognition (CVPR)*, pages 16000–16009, 2022. [1](#), [2](#), [5](#), [6](#), [7](#)
- [18] Zhicheng Huang, Xiaojie Jin, Chengze Lu, Qibin Hou, Ming-Ming Cheng, Dongmei Fu, Xiaohui Shen, and Jiashi Feng. Contrastive masked autoencoders are stronger vision learners. *arXiv preprint arXiv:2207.13532*, 2022. [6](#)
- [19] Richard M Karp, Umesh V Vazirani, and Vijay V Vazirani. An optimal algorithm for on-line bipartite matching. In *Proceedings of the twenty-second annual ACM symposium on Theory of computing*, pages 352–358, 1990. [2](#)
- [20] Simon Kornblith, Jonathon Shlens, and Quoc V Le. Do better imagenet models transfer better? In *Proceedings of the IEEE/CVF Conference on Computer Vision and Pattern Recognition (CVPR)*, pages 2661–2671, 2019. [8](#)
- [21] Gang Li, Heliang Zheng, Daqing Liu, Chaoyue Wang, Bing Su, and Changwen Zheng. Semmae: Semantic-guided masking for learning masked autoencoders. *arXiv preprint arXiv:2206.10207*, 2022. [6](#)
- [22] Xiaotong Li, Yixiao Ge, Kun Yi, Zixuan Hu, Ying Shan, and Ling-Yu Duan. mc-beit: Multi-choice discretization for image bert pre-training. In *European conference on computer vision*, 2022. [6](#)
- [23] Youwei Liang, Chongjian GE, Zhan Tong, Yibing Song, Jue Wang, and Pengtao Xie. EVit: Expediting vision transformers via token reorganizations. In *International Conference on Learning Representations*, 2022. [2](#)
- [24] S. Lloyd. Least squares quantization in pcm. *IEEE Transactions on Information Theory*, 28(2):129–137, 1982. [2](#)
- [25] Shlok Mishra, Joshua Robinson, Huiwen Chang, David Jacobs, Aaron Sarna, Aaron Maschinot, and Dilip Krishnan. A simple, efficient and scalable contrastive masked autoen-

- coder for learning visual representations. *arXiv preprint arXiv:2210.16870*, 2022. 6
- [26] Norman Mu, Alexander Kirillov, David Wagner, and Saining Xie. Slip: Self-supervision meets language-image pre-training. *arXiv preprint arXiv:2112.12750*, 2021. 12
- [27] Zizheng Pan, Bohan Zhuang, Haoyu He, Jing Liu, and Jianfei Cai. Less is more: Pay less attention in vision transformers. In *AAAI*, 2022. 2
- [28] Zhiliang Peng, Li Dong, Hangbo Bao, Qixiang Ye, and Furu Wei. BEiT v2: Masked image modeling with vector-quantized visual tokenizers. 2022. 1, 2, 5, 6, 12
- [29] Alec Radford, Jong Wook Kim, Chris Hallacy, A. Ramesh, Gabriel Goh, Sandhini Agarwal, Girish Sastry, Amanda Askell, Pamela Mishkin, Jack Clark, Gretchen Krueger, and Ilya Sutskever. Learning transferable visual models from natural language supervision. In *ICML*, 2021. 2, 5, 7, 12
- [30] Aditya Ramesh, Mikhail Pavlov, Gabriel Goh, Scott Gray, Chelsea Voss, Alec Radford, Mark Chen, and Ilya Sutskever. Zero-shot text-to-image generation. In *International Conference on Machine Learning*, pages 8821–8831. PMLR, 2021. 2
- [31] Yongming Rao, Wenliang Zhao, Benlin Liu, Jiwen Lu, Jie Zhou, and Cho-Jui Hsieh. Dynamicvit: Efficient vision transformers with dynamic token sparsification. *Advances in neural information processing systems*, 34:13937–13949, 2021. 2
- [32] Benjamin Recht, Rebecca Roelofs, Ludwig Schmidt, and Vaishaal Shankar. Do imagenet classifiers generalize to imagenet? In *International Conference on Machine Learning*, 2019. 2
- [33] Sucheng Ren, Fangyun Wei, Samuel Albanie, Zheng Zhang, and Han Hu. Deepmim: Deep supervision for masked image modeling. *arXiv preprint arXiv:2303.08817*, 2023. 2, 6
- [34] Olga Russakovsky, Jia Deng, Hao Su, Jonathan Krause, Sanjeev Satheesh, Sean Ma, Zhiheng Huang, Andrej Karpathy, Aditya Khosla, Michael Bernstein, Alexander C. Berg, and Li Fei-Fei. Imagenet large scale visual recognition challenge. *International Journal of Computer Vision*, 115(3):211–252, 2015. 3, 7, 8, 12
- [35] Yehui Tang, Kai Han, Yunhe Wang, Chang Xu, Jianyuan Guo, Chao Xu, and Dacheng Tao. Patch slimming for efficient vision transformers. In *Proceedings of the IEEE/CVF Conference on Computer Vision and Pattern Recognition*, pages 12165–12174, 2022. 2
- [36] Chenxin Tao, Xizhou Zhu, Weijie Su, Gao Huang, Bin Li, Jie Zhou, Yu Qiao, Xiaogang Wang, and Jifeng Dai. Siamese image modeling for self-supervised vision representation learning. In *Proceedings of the IEEE/CVF Conference on Computer Vision and Pattern Recognition (CVPR)*, pages 2132–2141, 2023. 6
- [37] Hugo Touvron, Matthieu Cord, Matthijs Douze, Francisco Massa, Alexandre Sablayrolles, and Herve Jegou. Training data-efficient image transformers & distillation through attention. In *International Conference on Machine Learning*, pages 10347–10357, 2021. 6
- [38] Hugo Touvron, Matthieu Cord, and Hervé Jégou. Deit iii: Revenge of the vit. In *Computer Vision—ECCV 2022: 17th European Conference, Tel Aviv, Israel, October 23–27, 2022, Proceedings, Part XXIV*, pages 516–533. Springer, 2022. 6
- [39] Hugo Touvron, Matthieu Cord, Maxime Oquab, Piotr Bojanowski, Jakob Verbeek, and Hervé Jégou. Co-training 21 submodels for visual recognition. In *Proceedings of the IEEE/CVF Conference on Computer Vision and Pattern Recognition (CVPR)*, pages 11701–11710, 2023. 6
- [40] Grant Van Horn, Oisín Mac Aodha, Yang Song, Yin Cui, Chen Sun, Alex Shepard, Hartwig Adam, Pietro Perona, and Serge Belongie. The inaturalist species classification and detection dataset. In *Proceedings of the IEEE/CVF Conference on Computer Vision and Pattern Recognition (CVPR)*, pages 8769–8778, 2018. 7, 8
- [41] Haochen Wang, Kaiyou Song, Junsong Fan, Yuxi Wang, Jin Xie, and Zhaoxiang Zhang. Hard patches mining for masked image modeling. In *Proceedings of the IEEE/CVF Conference on Computer Vision and Pattern Recognition (CVPR) (CVPR)*, 2023. 6
- [42] Chen Wei, Haoqi Fan, Saining Xie, Chao-Yuan Wu, Alan Yuille, and Christoph Feichtenhofer. Masked feature prediction for self-supervised visual pre-training. In *Proceedings of the IEEE/CVF Conference on Computer Vision and Pattern Recognition (CVPR)*, 2022. 6
- [43] Longhui Wei, Lingxi Xie, Wengang Zhou, Houqiang Li, and Qi Tian. Mvp: Multimodality-guided visual pre-training. In *European Conference on Computer Vision*, pages 337–353. Springer, 2022. 2, 6
- [44] Yixuan Wei, Han Hu, Zhenda Xie, Zheng Zhang, Yue Cao, Jianmin Bao, Dong Chen, and Baining Guo. Contrastive learning rivals masked image modeling in fine-tuning via feature distillation. *arXiv preprint arXiv:2205.14141*, 2022. 2, 6
- [45] Zhirong Wu, Zihang Lai, Xiao Sun, and Stephen Lin. Extreme masking for learning instance and distributed visual representations. *arXiv preprint arXiv:2206.04667*, 2022. 6
- [46] Tete Xiao, Yingcheng Liu, Bolei Zhou, Yuning Jiang, and Jian Sun. Unified perceptual parsing for scene understanding. In *European Conference on Computer Vision*. Springer, 2018. 7
- [47] Zhenda Xie, Zheng Zhang, Yue Cao, Yutong Lin, Jianmin Bao, Zhuliang Yao, Qi Dai, and Han Hu. Simmim: A simple framework for masked image modeling. In *International Conference on Computer Vision*, 2022. 1, 2, 6
- [48] Yifan Xu, Zhijie Zhang, Mengdan Zhang, Kekai Sheng, Ke Li, Weiming Dong, Liqing Zhang, Changsheng Xu, and Xing Sun. Evo-vit: Slow-fast token evolution for dynamic vision transformer. In *Proceedings of the AAAI Conference on Artificial Intelligence*, pages 2964–2972, 2022. 2
- [49] Kun Yi, Yixiao Ge, Xiaotong Li, Shusheng Yang, Dian Li, Jianping Wu, Ying Shan, and Xiaohu Qie. Masked image modeling with denoising contrast. *International Conference on Learning Representations*, 2023. 6
- [50] Bolei Zhou, Hang Zhao, Xavier Puig, Sanja Fidler, Adela Barriuso, and Antonio Torralba. Scene parsing through ade20k dataset. In *Proceedings of the IEEE/CVF Conference on Computer Vision and Pattern Recognition (CVPR)*, 2017. 7, 12, 14

- [51] Jinghao Zhou, Chen Wei, Huiyu Wang, Wei Shen, Cihang Xie, Alan Yuille, and Tao Kong. ibot: Image bert pre-training with online tokenizer. In *International Conference on Learning Representations*, 2022. [1](#), [2](#), [6](#)

# Masked Image Modeling via Dynamic Token Morphing

## Supplementary Material

This supplementary material includes additional experimental analyses of our proposed method. We first present additional examples of spatial inconsistency among patches from pre-trained models. Then, we verify the further applicability of Dynamic Token Morphing (DTM) on SSL framework beyond Masked Image Modeling methods and target models beyond CLIP [29]. Moreover, we conduct an ablation study on loss functions. Finally, we provide implementation details for both pre-training and fine-tuning on ImageNet-1K [34], as well as fine-tuning on ADE20K [50].

### A. More examples of spatial inconsistency

We further investigate the spatial inconsistency of patch representations generated by a pre-trained model across various samples. We visualize prediction results for each patch in the bounding boxes through patch-wise zero-shot classification with and without token morphing using CLIP [29]. Specifically, we color the patches in green or red to denote that the predicted classes are related or unrelated to the ground-truth class, respectively. Moreover, we gradually vary the lightness of the colors to exhibit the degree of similarity and dissimilarity. As shown in Fig. 6, patch representations without token morphing reveal spatially inconsistent patch-wise predictions compared to the prediction results with token morphing, which reveals the spatially inconsistent representations among patches. In addition, predictions with token morphing exhibit significantly more accurate patches compared to predictions without token morphing.

### B. Applicability on SLIP

We apply DTM with the SLIP [26] to verify its applicability to various target models. We compare fine-tuning accuracies of the baseline and our method pre-trained by target patches from SLIP. Specifically, we generate target tokens using SLIP along with its projector. We pre-train ViT-B/16 with a resolution of  $224 \times 224$  for 300 epochs and fine-tune for 100 epochs on ImageNet-1K [34]. As shown in Table 9, our DTM successfully improves the fine-tuning accuracy of the baselines pre-trained with SLIP by 0.5%p, which reveals its general applicability beyond CLIP [29].

### C. Ablation study on loss functions

We compare various loss functions for our method in Table 10. We pre-train ViT-B/16 with a resolution of  $224 \times 224$  for 100 epochs and fine-tune for 100 epochs on ImageNet-1K [34]. While all loss functions work well, the cosine dis-

| Target models | Method   | ViT-S       | ViT-B       | ViT-L       |
|---------------|----------|-------------|-------------|-------------|
| SLIP          | Baseline | 81.8        | 84.0        | 85.7        |
|               | DTM      | 82.1 (+0.3) | 84.5 (+0.5) | 86.1 (+0.4) |

Table 9. **Applicability of Dynamic Token Morphing (DTM) on SLIP.** We compare the fine-tuning accuracies between the baseline and our method pre-trained with SLIP [26], which is a more improved language-image pre-trained model. We observe that our method largely improves the fine-tuning performance, which showcases the applicability of our method beyond CLIP. We employ the ViT-B/16 architecture with a resolution of  $224 \times 224$ . All the models are pre-trained for 300 epochs.

| Case                  | FT. (%)     |
|-----------------------|-------------|
| $\ell_1$              | 83.2        |
| $\ell_2$              | 83.3        |
| Smoothed $\ell_1$     | 83.2        |
| Cosine distance (Cos) | <b>84.2</b> |

Table 10. **Ablation study on loss functions.** All the studies report fine-tuning accuracies for each configuration which are pre-trained with ViT-B/16. All the backbones are pre-trained for 100 epochs. While all the loss functions works, Cosine distance exhibits best performance, demonstrating that reducing normalized distances between corresponding morphed tokens is effective.

| Case                          | Throughput (image/s) | FT. (%)     |
|-------------------------------|----------------------|-------------|
| Baseline                      | <b>1460.0</b>        | 84.3        |
| Layer-wise K-Means clustering | 1265.4               | 85.1        |
| DTM (K-Means clustering)      | 489.1                | <b>85.4</b> |
| DTM (Bipartite matching)      | 1446.0               | <b>85.4</b> |

Table 11. **Ablation study on clustering algorithms.** We report fine-tuning accuracies and throughputs for each pre-training configuration with ViT-B/16. We compared DTM with Bipartite matching, DTM with K-Means clustering, and layer-wise K-Means clustering. For the layer-wise K-Means clustering, we use constant numbers of clusters and iterations. Our DTM methods outperform the baseline with large margins. Moreover, DTM with K-Means clustering surpasses layer-wise K-means clustering, demonstrating the superiority of DTM.

tance works best.

### D. Implementation details

**Pre-training on ImageNet-1K.** The pre-training recipe for DTM mainly follows the recipe of BEiT v2 [28]. Table 12 reports the implementation details for pre-training. We adopt the hyperparameters for ViT-B/16 and ViT-L/16 pre-training from BEiT v2. Specifically, we use layer scales of 0.1 and  $1 \times 10^{-5}$  for ViT-B/16 and ViT-L/16, respectively. We employ both relative positional embeddings and shared relative positional embeddings. The maximum gra-



Figure 6. **Visualization of spatial inconsistency using CLIP.** We present patch-wise prediction results of samples for zero-shot image classification to visualize the spatial inconsistent predictions among patches. For the given input images in (a), (b) and (c) visualize the predicted classes for each patch within bounding boxes through patch-wise zero-shot classification with and without token morphing, respectively. Specifically, we depict differences between the predicted classes and the ground-truth class by varying the lightness of red colors. We observe the prediction results of the morphed tokens are more likely to align with the input patches, leading to reducing the spatial inconsistency incurred by patch-wise predictions.

dent value is constrained to 3.0. We apply color jittering followed by random resizing and cropping for data augmentation. The hyperparameters for ViT-S/16 replicate the settings of ViT-B/16.

**Fine-tuning on ImageNet-1K.** The fine-tuning recipe for DTM mainly follows the standard supervised learning recipe for ViT. Specifically, we adopt commonly used values for RandAugment, Mixup, Cutmix, and Label Smoothing. On the other hand, we employ relative positional embeddings. Stochastic depth is applied with values of 0.1,

| Hyperparameters                       | Small Size | Base Size           | Large Size |
|---------------------------------------|------------|---------------------|------------|
| Layers                                | 12         | 12                  | 24         |
| Hidden size                           | 384        | 768                 | 1024       |
| FFN inner hidden size                 | 1536       | 3072                | 4096       |
| Attention heads                       | 6          | 12                  | 16         |
| Layer scale                           | 0.1        | 0.1                 | 1e-5       |
| Patch size                            |            | 16 × 16             |            |
| Relative positional embeddings        |            | ✓                   |            |
| Shared relative positional embeddings |            | ✓                   |            |
| Training epochs                       |            | 300                 |            |
| Batch size                            |            | 1024                |            |
| Adam $\beta$                          |            | (0.9, 0.98)         |            |
| Base learning rate                    |            | 1.5e-4              |            |
| Learning rate schedule                |            | Cosine              |            |
| Warmup epochs                         |            | 10                  |            |
| Gradient clipping                     |            | 3.0                 |            |
| Dropout                               |            | ✗                   |            |
| Drop path                             |            | 0                   |            |
| Weight decay                          |            | 0.05                |            |
| Data Augment                          |            | RandomResizeAndCrop |            |
| Input resolution                      |            | 224 × 224           |            |
| Color jitter                          |            | 0.4                 |            |

Table 12. Hyperparameters for pretraining on ImageNet-1K.

0.1, and 0.2 for ViT-S/16, ViT-B/16, and ViT-L/16, respectively. The overall recipe is detailed in Table 13.

**Fine-tuning on ADE20K.** Table 14 summarizes the fine-tuning recipe of ViT/16 for the semantic segmentation task on ADE20K [50]. We employ AdamW with momentum (0.9, 0.999) and warm-up for 1500 iterations. The learning rate is linearly scheduled with a value of  $5 \times 10^{-5}$ . We apply layer-wise learning rate decay of 0.75, stochastic depth of 0.1, and weight decay of 0.05. The model is fine-tuned using 8 V100-32GB GPUs.

| Hyperparameters                       | ViT-S/16 | ViT-B/16         | ViT-L/16 |
|---------------------------------------|----------|------------------|----------|
| Fine-tuning epochs                    | 300      | 100              | 50       |
| Warmup epochs                         | 10       | 10               | 5        |
| Layer-wise learning rate decay        | 0.6      | 0.6              | 0.8      |
| Batch size                            |          | 1024             |          |
| Adam $\epsilon$                       |          | 1e-8             |          |
| Adam $\beta$                          |          | (0.9, 0.999)     |          |
| Base learning rate                    |          | 5e-4             |          |
| Learning rate schedule                |          | Cosine           |          |
| Repeated Aug                          |          | $\times$         |          |
| Weight decay                          |          | 0.05             |          |
| Label smoothing $\epsilon$            |          | 0.1              |          |
| Stoch. depth                          | 0.1      | 0.1              | 0.2      |
| Dropout                               |          | $\times$         |          |
| Gradient clipping                     |          | $\times$         |          |
| Erasing prob.                         |          | 0.25             |          |
| Input resolution                      |          | $224 \times 224$ |          |
| Rand Augment                          |          | 9/0.5            |          |
| Mixup prob.                           |          | 0.8              |          |
| Cutmix prob.                          |          | 1.0              |          |
| Relative positional embeddings        |          | $\checkmark$     |          |
| Shared relative positional embeddings |          | $\times$         |          |

Table 13. Hyperparameters for fine-tuning on ImageNet-1K.

| Hyperparameters                       | ViT-B/16         |
|---------------------------------------|------------------|
| Input resolution                      | $512 \times 512$ |
| Peak learning rate                    | 5e-5             |
| Fine-tuning steps                     | 160K             |
| Batch size                            | 16               |
| Adam $\epsilon$                       | 1e-8             |
| Adam $\beta$                          | (0.9, 0.999)     |
| Layer-wise learning rate decay        | 0.75             |
| Minimal learning rate                 | 0                |
| Learning rate schedule                | Linear           |
| Warmup steps                          | 1500             |
| Dropout                               | $\times$         |
| Stoch. depth                          | 0.1              |
| Weight decay                          | 0.05             |
| Relative positional embeddings        | $\checkmark$     |
| Shared relative positional embeddings | $\times$         |

Table 14. Hyperparameters for fine-tuning on ADE20K.